

Quantum Face Recognition Protocol with Ghost Imaging

Vahid Salari,^{1,2,*} Dilip Paneru,³ Erhan Saglamyurek,^{4,5} Milad Ghadimi,⁶ Moloud Abdar,⁷
Mohammadreza Rezaee,³ Mehdi Aslani,⁶ Shabir Barzanjeh,⁵ and Ebrahim Karimi^{3,8,†}

¹BCAM - Basque Center for Applied Mathematics; Alameda de Mazarredo, 14,48009 Bilbao, Basque Country - Spain

²Department of Physics and Astronomy, Howard University, Washington DC, USA

³Department of physics, University of Ottawa, Advanced Research Complex, 25 Templeton Street, K1N 6N5, Ottawa, ON, Canada

⁴Department of Physics, University of Alberta, Edmonton, AB T6G 2E1, Canada

⁵Department of Physics and Astronomy, University of Calgary, Calgary, AB T2N 1N4 Canada

⁶Department of Physics, Isfahan University of Technology, Isfahan 8415683111, Iran

⁷Institute for Intelligent Systems Research and Innovation (IISRI), Deakin University, Australia

⁸National Research Council of Canada, 100 Sussex Drive, K1A 0R6, Ottawa, ON, Canada

(Dated: January 18, 2022)

Face recognition is one of the most ubiquitous examples of pattern recognition in machine learning, with numerous applications in security, access control, and law enforcement, among many others. Pattern recognition with classical algorithms requires significant computational resources, especially when dealing with high-resolution images in an extensive database. Quantum algorithms have been shown to improve the efficiency and speed of many computational tasks, and as such, they could also potentially improve the complexity of the face recognition process. Here, we propose a quantum machine learning algorithm for pattern recognition based on quantum principal component analysis (QPCA), and quantum independent component analysis (QICA). A novel quantum algorithm for finding dissimilarity in the faces based on the computation of trace and determinant of a matrix (image) is also proposed. The overall complexity of our pattern recognition algorithm is $O(N \log N) - N$ is the image dimension. As an input to these pattern recognition algorithms, we consider experimental images obtained from quantum imaging techniques with correlated photons, e.g. “interaction-free” imaging or “ghost” imaging. Interfacing these imaging techniques with our quantum pattern recognition processor provides input images that possess a better signal-to-noise ratio, lower exposures, and higher resolution, thus speeding up the machine learning process further. Our fully quantum pattern recognition system with quantum algorithm and quantum inputs promises a much-improved image acquisition and identification system with potential applications extending beyond face recognition, e.g., in medical imaging for diagnosing sensitive tissues or biology for protein identification.

INTRODUCTION

In any intelligent image processing system, there are essentially two main steps: the acquisition of the image and the recognition of the desired patterns. Image acquisition for any pattern recognition method can be performed in multiple ways. For instance, classical sources (incoherent light from thermal radiation or a coherent beam from a laser) or quantum sources (entangled photons obtained from down conversion or squeezed light) can be used to obtain the images. Classical bright field imaging techniques employing the former sources, have the disadvantage of high probe illumination requirement, especially while imaging sensitive samples. Additionally, they are also plagued by the shot noise inherent in the intensities, and the background noise from the environment. Quantum techniques such as quantum illumination, or ghost imaging or even interaction-free imaging, alleviates the problems of background noise, and the probe illumination by utilizing quantum correlations between photon pairs [1]. Furthermore, quantum sub-shot noise imaging [2] and super resolution techniques [3] enhance the noise sensitivity and resolution in any images beyond the classical limits.

As a second important step, pattern recognition in the acquired images is a prominent feature of any intelligent imaging system. Face recognition [4] is one of the branches of pattern recognition, with numerous applications such as face ID verification, passport checks, entrance control, computer access control, criminal investigations, crowd surveillance, and witness face reconstruction [5], among several others. For face recognition, several classical machine learning algorithms exist [6], generally requiring huge computational resources especially when faced with the problem of identification from a large database. Quantum machine learning algorithms employing quantum features such as superposition and entanglement [7–15] promise enhancements in terms of the computing resources and the speed compared to the classical counterparts. Several experimental researches have been done to implement these algorithms [16–21]. In this article, we present a quantum algorithm for face recognition as one of the potential applications of quantum algorithms in machine learning.

The problem of identification of faces from any images generally constitutes different steps (shown in Figure 1): creating a database of faces consisting of training and test images, feature extraction using principal component analysis (PCA), linear discriminant analysis (LDA) or independent component analysis (ICA), feature matching using dissimilarity measures, and recognition [22]. PCA extracts the eigenstates (or eigenfaces) of the covariance matrix of the images

* vsalari@bcmath.org

† ekarimi@uottawa.ca

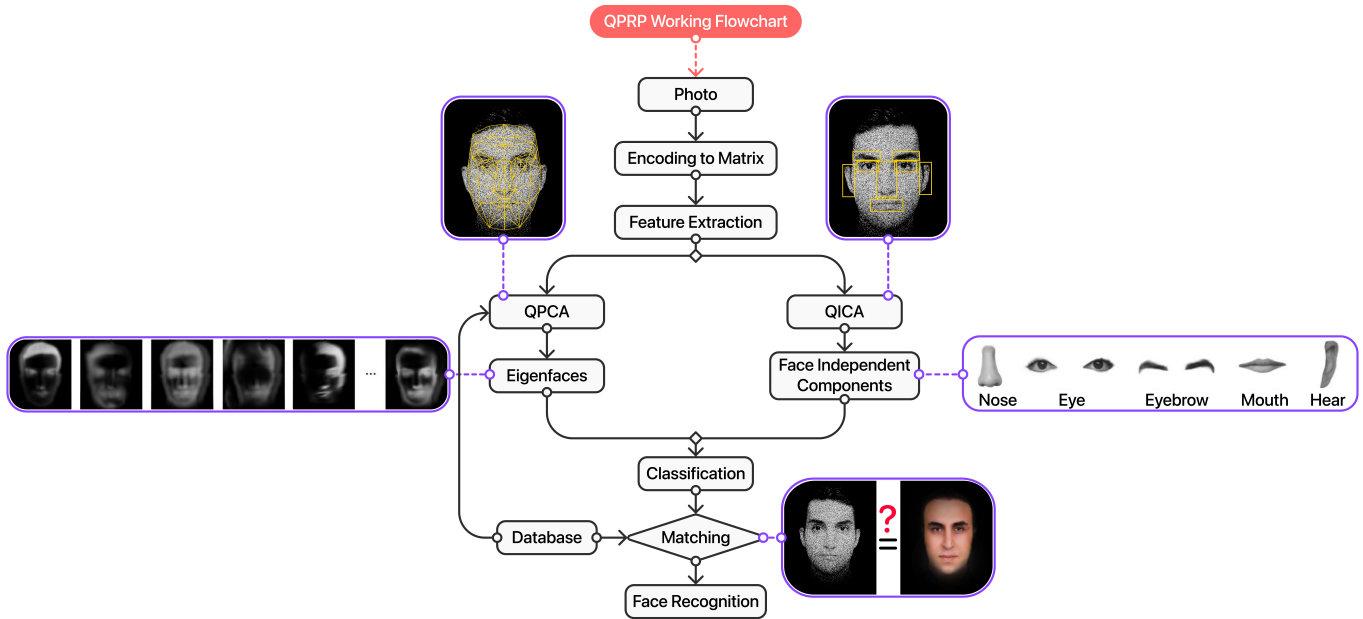


FIG. 1. **Flowchart of the quantum algorithm for face recognition.** The quantum algorithm is proposed to be performed in a quantum processor, which we call it quantum pattern recognition processor (QPRP). First the image is converted into matrix form, on which feature extraction algorithms such as quantum principal component analysis (QPCA) or quantum independent component analysis (QICA) are applied. QPCA extracts the eigenstates (or eigenfaces) of the covariance matrix of the images in the database. The eigenfaces include information like average face, gender (male, female), face direction, brightness, shadows, etc. QICA extracts the independent elements such as eyes, eyebrows, mouth, nose, etc. in a face. The complexity of this stage is $O(\log N) - N$ is the dimension of the image. Then, the given faces are compared with the faces in the database by using dissimilarity measure based on the log determinant divergence, and the best match among the faces in the database is identified.

in the database, including information like average face, gender (male or female), face direction, brightness, shadows, etc. ICA, however, extracts the independent elements such as eyes, eyebrows, mouth, nose, etc. in a face. Quantum algorithms which provide speedup for PCA and ICA have already been proposed [7, 23]. Here, we focus on three main steps: (1) Quantum Principle Component Analysis (QPCA) [7], (2) Quantum Independent Component Analysis (QICA) [23], and (3) Dissimilarity measures (i.e., face matching), to develop a quantum algorithm for face recognition. In what follows, we present a quantum algorithm for dissimilarity measures for face matching with speedup. This is based on a quantum algorithm to compute the log determinant divergence using both the determinant and the trace of a matrix. Our algorithm combined with the inputs obtained from quantum imaging techniques provides a fully intelligent pattern identification system, with the joint benefit of the low-dose and higher resolution of quantum imaging methods, and the speedup and efficiency of the quantum algorithms. Figure 1 shows the flowchart of the quantum algorithm for the pattern identification.

QUANTUM FACE RECOGNITION

Classical algorithms are unable to process quantum data directly. During the conversion of the quantum states (qu-

bits) to classical data (bits), most of the information is lost in the measurement process, due to the “collapse” of the wavefunction. Although techniques such as quantum state tomography implemented on unlimited ensemble of the states can be used to fully reconstruct the quantum states from classical projections, these processes are generally complex and expensive. Therefore, the optimal input to our quantum algorithms, would be the quantum states directly obtained from quantum processes, for example, quantum imaging methods, or from a quantum memory, without performing a strong measurement on the wavefunction.

Photonic quantum memories [24], allowing storage and on-demand retrieval of quantum states of light, is one of the key components for the realization of quantum optical pattern-recognition technology. Quantum memories essentially form a quantum database for the matching stage in the recognition process. With the state-of-art quantum memories, the possibility of storing hundreds of spatial modes has already been shown in experimental studies using atomic-cold gases [25, 26]. Furthermore, using solid-state atomic memories, it is possible to simultaneously store hundreds of photonic quantum states in distinct temporal modes, thus allowing us to store patterns scanned at separate times [27, 28]. In addition, optically accessible spin-states of certain atomic systems can reach several hours of coherence time [29]. A very recent experimental demonstration reports one-hour memory lifetime for light storage, showing the feasibility of long-lived

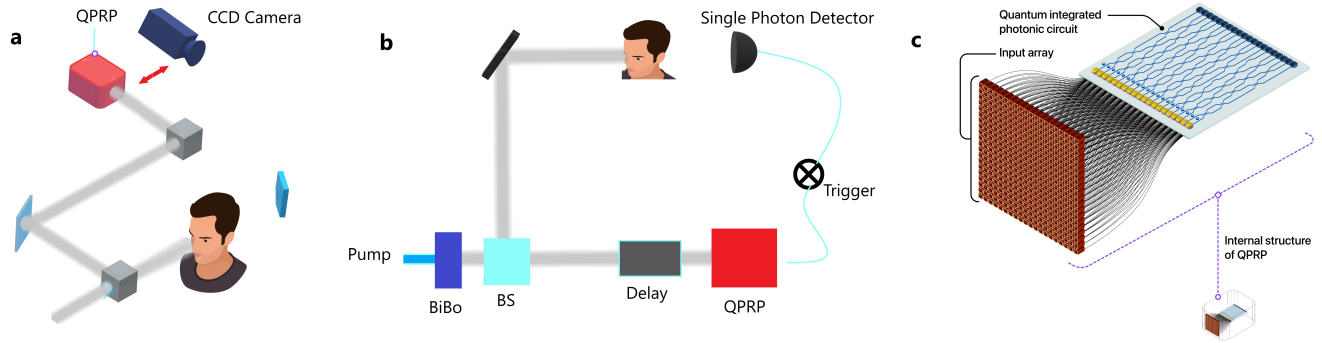


FIG. 2. **Intelligent pattern recognition in quantum imaging.** Data from quantum imaging methods such as (a) Interaction Free Imaging and (b) Ghost Imaging act as an input to (c) Quantum Pattern Recognition Processor (QPRP). The latter, i.e., QPRP, applies quantum machine learning to find the patterns in the database.

photonic quantum memory devices [30]. Atomic memory approaches have also been shown to reach high retrieval efficiencies up to 92% [31] and high fidelities above 99% [32]. However, an implementation with all of the aforementioned properties still remains as a challenge in developing a practical quantum database memory.

Quantum techniques such as quantum ghost imaging [33], quantum lithography [34], or quantum sensing [35], when appropriately interfaced with photonic quantum processors, for example an array of optical fibers connected to an integrated quantum photonic circuit, can also act as inputs to our algorithms (see Figure 2). Here for the case of our face recognition algorithm, we assume that the input images are acquired by quantum ghost imaging [33]. Ghost imaging exploits the spatial correlations between photon pairs generated through a nonlinear process called spontaneous parametric down-conversion (SPDC). Since the images are obtained by triggering the shutter in order to capture only the “coincident” photon pairs, the level of background noise is significantly reduced, along with a reduction in probe illumination. In a variation of this technique using non degenerate photon pairs, the image detection and sample interaction can happen at different wavelengths, which can be useful when imaging sensitive tissues when limited in detection technologies [36]. Combining quantum detection techniques such as interaction-free measurement with ghost imaging, the illumination level required for the same levels of Signal to Noise ratio (SNR) in images [37] is further reduced significantly. Figure 3 shows some of the images of human faces obtained in a quantum ghost imaging setup, where spatially correlated photon pairs (namely signal and idler), are generated by pumping a BiBo crystal with pump photons. Phase holograms placed in a Spatial Light Modulator, a liquid crystal device, created by superimposing the human faces with a diffraction grating acts as an object for the signal photon, while the idler photon passes to the Intensified Charged Coupled Devices (ICCD) camera via a delay line. The images are obtained by triggering the ICCD shutter with the signal photons detected through a Single Pho-

ton Avalanche Diode (SPAD) detector – see Supplementary Information (SI) for the detail of the experimental setup.

A. Quantum principal component analysis (QPCA)

We have now the input images either retrieved from a quantum memory or directly as outputs from a quantum imaging setup. The pattern recognition processor applies Quantum Principal Component Analysis (QPCA) [7, 38] to extract the principal eigenvectors of the covariance matrix C_X , formed by the set of the training images.

Let us consider a set of N -dimensional training images (or faces), $\{|x^{(1)}\rangle, \dots, |x^{(M)}\rangle\}$. Here, $|x^{(i)}\rangle$ is the i -th training image, which is given by,

$$|x^{(i)}\rangle = \sum_{q=1}^N x_q^{(i)} |\psi_q^{(i)}\rangle, \quad (1)$$

where $x_q^{(i)}$ are the components, and $|\psi_q^{(i)}\rangle$ are the basis kets. The covariance matrix C_X can be formed as a sum over M training faces [38],

$$C_X = \frac{1}{M} \sum_{i=1}^M |x^{(i)}\rangle \langle x^{(i)}|. \quad (2)$$

The next step is to exponentiate the covariance matrix C_X , so that we can use the Quantum Phase Estimation (QPE) subroutine for finding the eigenvectors and eigenvalues. It has been shown that the exponentiation of the covariance matrix, i.e., $e^{-iC_X t}$, can be performed in $\mathcal{O}(\log N)$ time [7].

In QPCA algorithm, for the phase estimation subroutine, we apply the operator $U = e^{-iC_X t}$ on C_X [38]. The action of U on one of the states $|x^{(i)}\rangle$ in C_X is:

$$e^{-iC_X t} |x^{(i)}\rangle \rightarrow \sum_{j=1}^M c^{(ij)} |\phi^j\rangle, \quad (3)$$

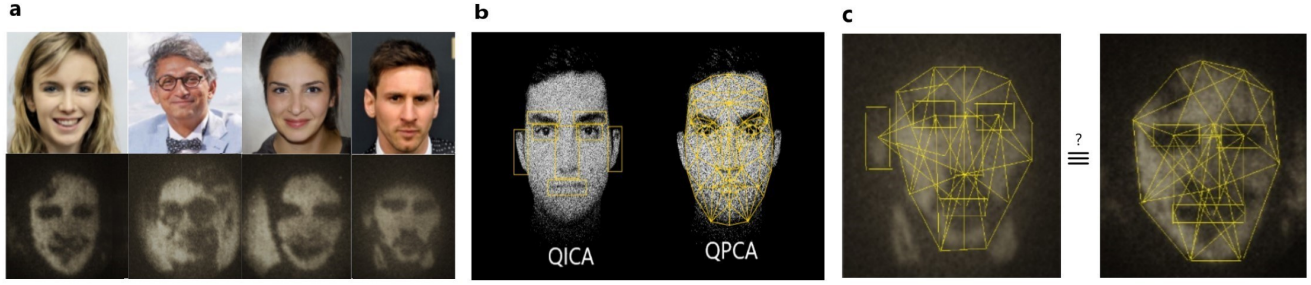


FIG. 3. **Face recognition in ghost images.** (a) Images of the original human faces (top) and the corresponding experimental ghost images (bottom) obtained in a ghost imaging setup. A femtosecond laser is used to generate spatially entangled photon pairs. One of the photons illuminates a spatial light modulator, which imprints different images onto the photon, and can act as a trigger for the other photon that was detected by an intensified CCD camera. (b) Quantum Independent Component Analysis (QICA), and Quantum Principal Component Analysis (QPCA), of the faces to detect the independent components, and principal features in the faces. (c) Dissimilarity measure between the ghost images with the images in the database for their identification.

where $|\phi^j\rangle$'s are the eigenvectors of C_X , and $c^{ij} = e^{-i\tilde{\lambda}_c^{(j)}t}\langle\phi^j|x^{(i)}\rangle$ in which $\tilde{\lambda}_c^{(j)} = (2\pi\lambda_c^{(j)}t)/2^n$ where $\lambda_c^{(j)}$'s are the corresponding estimated eigenvalues of C_X with precision n [7, 38].

In order to obtain the principal eigenfaces (the eigenvectors of the covariance matrix with larger eigenvalues), we define a score $s^{(ij)}$, which is the projection of an eigenvector $|\phi^j\rangle$ on a training vector $|x^{(i)}\rangle$,

$$s^{(ij)} = \langle x^i | \phi^j \rangle = \sum_{q=1}^N x_q^{(i)} \phi_q^{(j)}, \quad (4)$$

where $\phi_n^{(j)}$ are the components of the eigenvector $|\phi^j\rangle$. The eigenvectors corresponding to the r highest scores are the principal components (or eigenfaces). Each face can be expanded in terms of the r eigenfaces (principal components) but with different weights ω_j 's as follows

$$|\text{Face}^{(i)}\rangle = \sum_{j=1}^r \omega_j |\phi^j\rangle. \quad (5)$$

The “mean image” is the eigenface corresponding to the largest eigenvalue of C_X . The QPCA algorithm is efficient for the case $r \ll N$ [38].

B. Quantum independent component analysis (QICA)

In classical machine learning, Independent Component Analysis (ICA) is performed to decompose an observed signal into a linear combination of unknown independent signals [22]. Similar to the PCA, the ICA finds a new basis to represent the data, however with a different goal. We assume that there is a data set of faces $s \in R^d$ that is a collection of d independent elements in the face such as nose, eye, eyebrow, mouth, etc. Each image observed through a camera can

be expressed as $x = F \cdot s$, where F is a mixing matrix of the independent face elements. Repeated observation gives us a dataset x as $\{x^{(i)}, \dots, x^{(M)}\}$, and ICA estimates the independent sources $s^{(i)}$ that had generated the face. We let $W = F^{-1}$ which is the unmixing matrix and solve the linear systems of equations $s^{(i)} = W x^{(i)}$ for estimating the independent elements of the face. We should note here that $s^{(i)}$ is a d -dimensional vector and $s_j^{(i)}$ is the data of element j . Similarly, $x^{(i)}$ is a d -dimensional vector, and $x_j^{(i)}$ is the observed (or recorded) element j by camera. The ICA can be exponentially speedup via a quantum algorithm for sparse matrices, with the Harrow-Hassidim-Lloyd (HHL) algorithm [23], which is used to solve linear systems of equations optimally with $O(\log N)$. For comparison, classically it takes a time $O(N^3)$ to be solved via the Gauss elimination, and approximately $O(N\sqrt{\kappa})$ via iterative methods [23] for a sparse matrix of size $N \times N$, with κ being the ratio between the greatest and the smallest eigenvalue.

C. Pattern matching: Comparing Faces

As important details of a face are obtained either by using QPCA or QICA, each face is represented in the form of a sparse matrix in which non-important elements are set to zero. The last and important step of the algorithm is comparing the face patterns to recognize the target face. Pattern matching algorithms investigate exact matches in the input with pre-existing patterns in the database. In fact, the problem here is comparing matrices with each other. The evaluation of matching between matrices (or face patterns) can be done by using “dissimilarity” [39] measures that calculate the “distance” between the matrices. The lower the values of the dissimilarity/distance measures, more similar the matrices, with the fully matched matrices having a zero distance. One such distance measure used to compare two matrices X and Y is

called the ‘‘Log-determinant divergence’’ [39, 40] defined as,

$$D(X, Y) = \text{Tr}(X \cdot Y^{-1}) - \log \det(X \cdot Y^{-1}) - N, \quad (6)$$

where N is the dimension of the matrices. When $D = 0$, the matrices X and Y are completely matched, and higher the distance value the more different are the matrices. The least value among the all distance values identifies the best match and consequently recognizes the face. As it is seen in the distance formula, it is a benefit to be able to calculate the trace and the determinants of matrices with speedup to expedite the distance calculation. In the following, we propose quantum algorithms for computation of the determinant and the trace of a sparse matrix.

Quantum Computation of Sparse Matrix Determinants and Trace: To obtain a measure of dissimilarity between two matrices we need to calculate the determinant and the trace of the sparse matrix $A = X \cdot Y^{-1}$. First we calculate Y^{-1} using the HHL algorithm [23] and obtain A by multiplying it with X . We then apply the Quantum Phase Estimation (QPE) subroutine, which consists of a quantum Fourier transform (QFT) followed by a controlled Unitary (CU) operation, with $U = e^{-iAt}$, and an inverse quantum Fourier transform. We then apply a controlled Rotation operation followed by the inverse Quantum Phase Estimation (QPE) subroutine. At the end we have a multiplication operator Π which finally gives us the product of the eigenvalues – the algorithm steps are explained in more detail in the Supplementary Information. The running time of the algorithm up to the third step, i.e. applying the controlled-U operator, is $O(\log N(s^2\kappa^2/\epsilon))$ [23], where s is the sparsity, κ is the ratio of largest eigenvalue to the smallest eigenvalue of A , and ϵ is the acceptable error. Additionally, the multiplication operation in the last step can be performed in time $O(\log N)$ and the algorithm should run N times. Therefore, the overall complexity of the algorithm is $O(N \log N(1 + s^2\kappa^2/\epsilon))$, which is much faster than the classical ones (see Table I).

TABLE I. A Comparison of complexities between the classical approaches and our quantum approach, current work (CW), for the computation of determinant.

Approach	Method	Complexity	Ref.
Classic	Laplace	N^3	[41]
Classic	Gaussian	N^3	[41]
Classic	Coppersmith-Winograd	$N^{2.373}$	[42]
Classic	Wiedemann	$N^2 \log N$	[43]
Quantum	Our method	$N \log N$	CW

In order to compute the trace of the matrix A , an adder quantum algorithm [44] can speedup the computation. The adder operation between two diagonal elements is mainly based on the quantum Fourier transform (QFT), i.e. $|\Phi(a)\rangle := \text{QFT}|a\rangle = \frac{1}{\sqrt{N}} \sum_{k=0}^{N-1} e^{i\frac{2\pi ak}{N}} |k\rangle$ and the inverse QFT, i.e., $\text{QFT}^{-1}|\Phi(a)\rangle = |a\rangle$. By continuation of this method sequentially for the all diagonal elements, one can obtain the trace of the matrix. The detail of the adder algorithm and the quantum

circuit for the computation of trace is discussed in the Supplementary Information (Figure S2 shows the corresponding quantum circuit). The whole process which is based on QFT and QFT^{-1} has a complexity of $O(\log N)$.

TABLE II. Summary of estimated complexities in quantum face recognition algorithm.

Method	Output	Complexity	Ref.
QPCA	Eigenfaces	$\log N$	[7]
QICA & HHL	Face components	$\log N$	[23]
HHL	Matrix inversion	$\log N$	[23]
Our method	Determinant calculation	$N \log N$	CW
Our method	Trace calculation	$\log N$	CW
Log-det divergence	Face matching	$N \log N$	CW
Our method (General)	Face recognition	$N \log N$	CW

QPCA and QICA both have logarithmic complexities, i.e., $O(\log N)$. For the calculation of the log determinant divergence, the computation of trace has a complexity of $O(\log N)$, while the determinant has complexity of $O(N \log N)$. Hence, the overall complexity of the whole algorithm is $O(N \log N)$. Table II shows a summary of estimated complexities along with the complexity of the general quantum face recognition algorithm.

CONCLUSION

In summary, we propose a new concept of a quantum protocol for 2D face recognition, combining the benefits of quantum imaging in image acquisition with the speedup from the quantum machine learning algorithms. In this concept, we consider images to be obtained via a ghost imaging protocol either as inputs to the quantum memories or as a hardware encoding of quantum information for the photonic pattern recognition processor. Feeding the ‘‘images’’ directly from a quantum protocol also eliminates the need for the conversion of classical data to quantum inputs for the processor saving valuable computational resources. The quantum pattern recognition processor then runs an algorithm composed of three main subroutines: (1) quantum principal components analysis (QPCA), (2) quantum independent component analysis (QICA), and (3) quantum dissimilarity measures for comparing faces. For the QPCA and QICA, we propose slight modifications in the existing algorithms, whereas for finding the dissimilarity measure, we propose a novel algorithm for obtaining the distance between two matrices based upon a metric called log-determinant divergence. Our algorithm obtains the determinant and the trace of the two matrices in $O(N \log N)$ time – N is the dimension of the matrix. Complexity analysis shows that all of the three parts have speedup as compared to their classical counterparts, with the overall complexity given by $O(N \log N)$. Our conceptual protocol provides a framework for an intelligent and fully quantum image recognition system with quantum inputs and a quantum machine learning processor. The joint benefits of the quantum image acquisition and quantum machine learning promises exciting technological developments in the field of image recognition systems.

- [1] Jeffrey H Shapiro and Robert W Boyd, “The physics of ghost imaging,” *Quantum Information Processing* **11**, 949–993 (2012).
- [2] Giorgio Brida, Marco Genovese, and I Ruo Berchera, “Experimental realization of sub-shot-noise quantum imaging,” *Nature Photonics* **4**, 227–230 (2010).
- [3] Mankei Tsang, Ranjith Nair, and Xiao-Ming Lu, “Quantum theory of superresolution for two incoherent optical point sources,” *Physical Review X* **6**, 031033 (2016).
- [4] et al. J. Wright, “Robust face recognition via sparse representation,” *IEEE Trans. Patt. Anal. Mach. Intell.* **31**, 210 (2009).
- [5] A. Acan O. Toygar, “Face recognition using pca, lda and ica approaches on colored images,” *J. Elect. Eng.* **3**, 735 (2003).
- [6] Md Khaled Hasan, Md Ahsan, SH Newaz, Gyu Myoung Lee, *et al.*, “Human face detection techniques: A comprehensive review and future research directions,” *Electronics* **10**, 2354 (2021).
- [7] Seth Lloyd, Masoud Mohseni, and Patrick Rebentrost, “Quantum principal component analysis,” *Nature Physics* **10**, 631–633 (2014).
- [8] Patrick Rebentrost, Masoud Mohseni, and Seth Lloyd, “Quantum support vector machine for big data classification,” *Physical review letters* **113**, 130503 (2014).
- [9] Seth Lloyd, Silvano Garnerone, and Paolo Zanardi, “Quantum algorithms for topological and geometric analysis of data,” *Nature communications* **7**, 1–7 (2016).
- [10] Jacob Biamonte, Peter Wittek, Nicola Pancotti, Patrick Rebentrost, Nathan Wiebe, and Seth Lloyd, “Quantum machine learning,” *Nature* **549**, 195–202 (2017).
- [11] F. Petruccione M. Schuld, *Supervised Learning with Quantum Computers*, 3rd ed., 10, Vol. 4 (Springer International Publishing, The address, 1993).
- [12] Devin Powell, “Quantum boost for artificial intelligence,” *Nature News* (2013).
- [13] G Alvarado Barrios, F Albarrán-Arriagada, FA Cárdenas-López, G Romero, and JC Retamal, “Role of quantum correlations in light-matter quantum heat engines,” *Physical Review A* **96**, 052119 (2017).
- [14] Francisco A Cárdenas-López, Lucas Lamata, Juan Carlos Retamal, and Enrique Solano, “Multiqubit and multilevel quantum reinforcement learning with quantum technologies,” *PloS one* **13**, e0200455 (2018).
- [15] Dilip Paneru, Eliahu Cohen, Robert Fickler, Robert W Boyd, and Ebrahim Karimi, “Entanglement: quantum or classical?” *Reports on Progress in Physics* **83**, 064001 (2020).
- [16] David Collins, Ki Wook Kim, William C Holton, Hanna Sierzputowska-Gracz, and EO Stejskal, “Nmr quantum computation with indirectly coupled gates,” *Physical Review A* **62**, 022304 (2000).
- [17] N Schuch and J Siewert, “Implementation of the four-bit deutsch–jozsa algorithm with josephson charge qubits,” *physica status solidi (b)* **233**, 482–489 (2002).
- [18] Zhen Wu, Jun Li, Wenqiang Zheng, Jun Luo, Mang Feng, and Xinhua Peng, “Experimental demonstration of the deutsch–jozsa algorithm in homonuclear multispin systems,” *Physical Review A* **84**, 042312 (2011).
- [19] Shigeki Takeuchi, “Experimental demonstration of a three-qubit quantum computation algorithm using a single photon and linear optics,” *Physical review A* **62**, 032301 (2000).
- [20] Stephan Gulde, Mark Riebe, Gavin PT Lancaster, Christoph Becher, Jürgen Eschner, Hartmut Häffner, Ferdinand Schmidt-Kaler, Isaac L Chuang, and Rainer Blatt, “Implementation of the deutsch–jozsa algorithm on an ion-trap quantum computer,” *Nature* **421**, 48–50 (2003).
- [21] Stefanie Barz, Ivan Kassal, Martin Ringbauer, Yannick Ole Lipp, Borivoje Dakić, Alán Aspuru-Guzik, and Philip Walther, “A two-qubit photonic quantum processor and its application to solving systems of linear equations,” *Scientific reports* **4**, 1–5 (2014).
- [22] Bruce A Draper, Kyungim Baek, Marian Stewart Bartlett, and J Ross Beveridge, “Recognizing faces with pca and ica,” *Computer vision and image understanding* **91**, 115–137 (2003).
- [23] Aram W Harrow, Avinatan Hassidim, and Seth Lloyd, “Quantum algorithm for linear systems of equations,” *Physical review letters* **103**, 150502 (2009).
- [24] Alexander I Lvovsky, Barry C Sanders, and Wolfgang Tittel, “Optical quantum memory,” *Nature photonics* **3**, 706–714 (2009).
- [25] Michał Parniak, Michał Dkabrowski, Mateusz Mazelanik, Adam Leszczyński, Michał Lipka, and Wojciech Wasilewski, “Wavevector multiplexed atomic quantum memory via spatially-resolved single-photon detection,” *Nature communications* **8**, 1–9 (2017).
- [26] YF Pu, N Jiang, W Chang, HX Yang, C Li, and LM Duan, “Experimental realization of a multiplexed quantum memory with 225 individually accessible memory cells,” *Nature communications* **8**, 1–6 (2017).
- [27] M Bonarota, JL Le Gouët, and T Chaneliere, “Highly multi-mode storage in a crystal,” *New Journal of Physics* **13**, 013013 (2011).
- [28] Jian-Shun Tang, Zong-Quan Zhou, Yi-Tao Wang, Yu-Long Li, Xiao Liu, Yi-Lin Hua, Yang Zou, Shuang Wang, De-Yong He, Geng Chen, *et al.*, “Storage of multiple single-photon pulses emitted from a quantum dot in a solid-state quantum memory,” *Nature communications* **6**, 1–7 (2015).
- [29] Manjin Zhong, Morgan P Hedges, Rose L Ahlefeldt, John G Bartholomew, Sarah E Beavan, Sven M Wittig, Jevon J Longdell, and Matthew J Sellars, “Optically addressable nuclear spins in a solid with a six-hour coherence time,” *Nature* **517**, 177–180 (2015).
- [30] Yu Ma, You-Zhi Ma, Zong-Quan Zhou, Chuan-Feng Li, and Guang-Can Guo, “One-hour coherent optical storage in an atomic frequency comb memory,” *Nature communications* **12**, 1–6 (2021).
- [31] Ya-Fen Hsiao, Pin-Ju Tsai, Hung-Shiue Chen, Sheng-Xiang Lin, Chih-Chiao Hung, Chih-Hsi Lee, Yi-Hsin Chen, Yong-Fan Chen, A Yu Ite, and Ying-Cheng Chen, “Highly efficient coherent optical memory based on electromagnetically induced transparency,” *Physical review letters* **120**, 183602 (2018).
- [32] Chao Liu, Zong-Quan Zhou, Tian-Xiang Zhu, Liang Zheng, Ming Jin, Xiao Liu, Pei-Yun Li, Jian-Yin Huang, Yu Ma, Tao Tu, *et al.*, “Reliable coherent optical memory based on a laser-written waveguide,” *Optica* **7**, 192–197 (2020).
- [33] Peter A Morris, Reuben S Aspden, Jessica EC Bell, Robert W Boyd, and Miles J Padgett, “Imaging with a small number of photons,” *Nature communications* **6**, 1–6 (2015).
- [34] Agedi N Boto, Pieter Kok, Daniel S Abrams, Samuel L Braunstein, Colin P Williams, and Jonathan P Dowling, “Quantum interferometric optical lithography: exploiting entanglement to beat the diffraction limit,” *Physical Review Letters* **85**, 2733 (2000).

- [35] Yonatan Israel, Shamir Rosen, and Yaron Silberberg, “Super-sensitive polarization microscopy using noon states of light,” *Physical review letters* **112**, 103604 (2014).
- [36] Kam Wai Clifford Chan, Malcolm N O’Sullivan, and Robert W Boyd, “Two-color ghost imaging,” *Physical Review A* **79**, 033808 (2009).
- [37] Yingwen Zhang, Alicia Sit, Frédéric Bouchard, Hugo Larocque, Florence Grenapin, Eliahu Cohen, Avshalom C Elitzur, James L Harden, Robert W Boyd, and Ebrahim Karimi, “Interaction-free ghost-imaging of structured objects,” *Optics express* **27**, 2212–2224 (2019).
- [38] Dawid Kopczyk, “Quantum machine learning for data scientists,” arXiv preprint arXiv:1804.10068 (2018).
- [39] Andrzej Cichocki, Sergio Cruces, and Shun-ichi Amari, “Log-determinant divergences revisited: Alpha-beta and gamma log-det divergences,” *Entropy* **17**, 2988–3034 (2015).
- [40] Inderjit S Dhillon and Joel A Tropp, “Matrix nearness problems with bregman divergences,” *SIAM Journal on Matrix Analysis and Applications* **29**, 1120–1146 (2008).
- [41] James R Bunch and John E Hopcroft, “Triangular factorization and inversion by fast matrix multiplication,” *Mathematics of Computation* **28**, 231–236 (1974).
- [42] Virginia Vassilevska Williams, “Multiplying matrices in $O(n^2 \cdot 373)$ time,” preprint (2014).
- [43] Douglas Wiedemann, “Solving sparse linear equations over finite fields,” *IEEE transactions on information theory* **32**, 54–62 (1986).
- [44] Lidia Ruiz-Perez and Juan Carlos Garcia-Escartin, “Quantum arithmetic with the quantum fourier transform,” *Quantum Information Processing* **16**, 152 (2017).

Acknowledgments: V. S. is very thankful for several helpful discussions with Mikel Sanz and Enrique Solano during his research stay in QUTIS center in Bilbao (Spain) and QuArtist center in Shanghai (China), both leading by Enrique Solano who encouraged the idea to be developed. Also, V. S. is very grateful for useful discussions with Seth Lloyd and Nathan Wiebe during the Quantum Machine Learning and Biomimetic Quantum Technologies conference held in Bilbao.

Funding: D. P., M. R. and E. K. acknowledge the support of Ontario’s Early Researcher Award (ERA), Canada Research Chairs (CRC), and the European Union’s Horizon 2020 Research and Innovation Programme (Q-SORT), grant number 766970. V. S. is grateful for the financial support by the Spanish State Research Agency through BCAM Severo Ochoa excellence accreditation SEV-2017-0718 and BERC 2018-2021 program. S.B. acknowledges funding by the Natural Sciences and Engineering Research Council of Canada (NSERC) through its Discovery Grant, funding and advisory support provided by Alberta Innovates through the Accelerating Innovations into CarE (AICE) – Concepts Program, and support from Alberta Innovates and NSERC through Advance Grant.

Author contributions: V.S. and D.P. contributed equally to this work. V.S. and E.K. developed the idea and consulted it with D.P., S.B., M.R., and E.S. to design the protocol. V.S., M.G., and M.Ab. developed the algorithm, D.P. performed the experiments under the supervision of E.K. All authors contributed to discussions. V.S., D.P., and E.K. wrote the

manuscript, and V.S., S.B., and E.K. revised the final version.

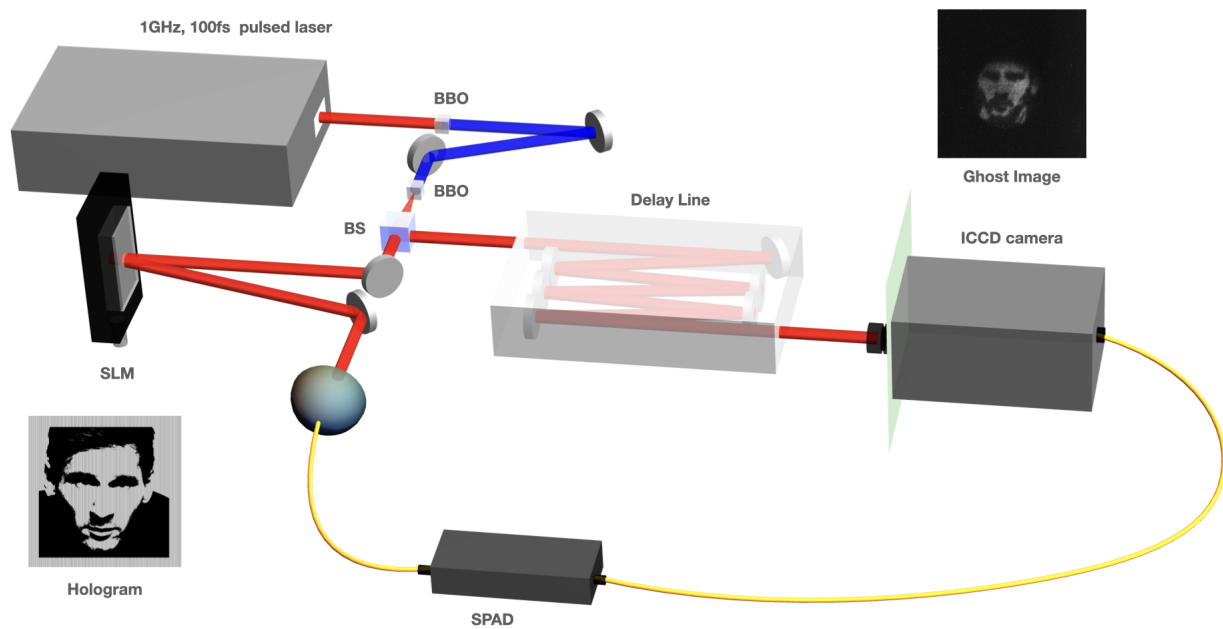
Competing interests: The authors declare that they have no competing interests.

Data and materials availability: All data needed to evaluate the conclusions in the paper are present in the paper and/or the Supplementary Materials. Additional data related to this paper may be requested from the authors.

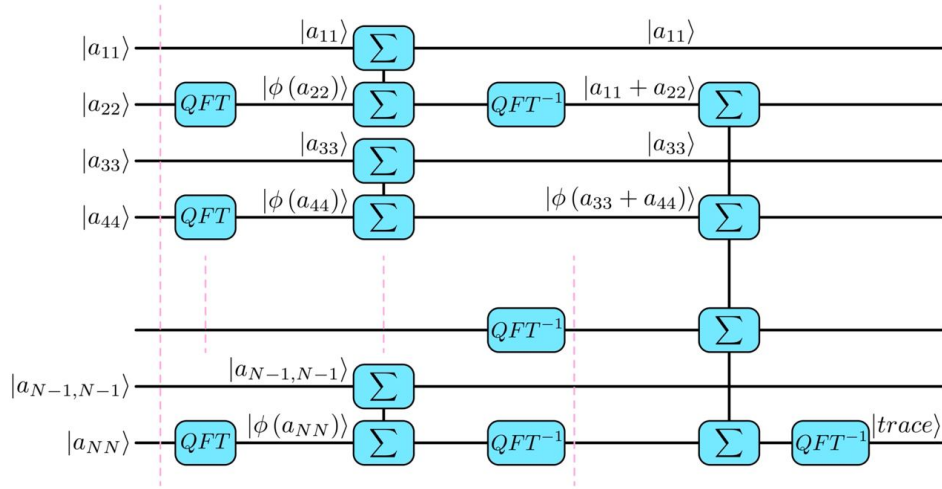
Supplementary Information for: Quantum Face Recognition Protocol with Ghost Imaging

S1. QUANTUM IMAGING

We elaborate on the experimental details of the image acquisition for the quantum pattern recognition protocol. Spatially correlated photon pairs, usually called signal and idler photons, are generated from a Spontaneous Parametric Down Conversion Process (SPDC) by pumping a nonlinear crystal. Utilizing the position and momentum correlations in these down converted photon pairs, one can non-locally obtain an image of an object that interacted only with the idler photons. The experimental setup we use is similar to a conventional ghost-imaging setup, see Fig. S1, with our object being a hologram placed in a Spatial Light Modulator (SLM), a liquid crystal device. We use a 1 GHz, 100 fs pulsed laser to pump a nonlinear crystal, β -Barium Borate (BBO), for generating a second harmonic output. We then use the second harmonic beam to pump a Type-I bismuth triborate (BiBO) crystal for the down conversion of photon pairs. The generated signal and idler pairs are split into two paths, i.e. the object arm (idler) and the camera arm (signal), via a 50:50 Beamsplitter (BS). The idler photon interacts with the SLM, on which we display the holograms created by superimposing the original face image with a diffraction grating. The grating sends only the desired photons from the incident beam to the first order, which then are coupled to a Single Mode Fibre (SMF) and sent into a Single Photon Avalanche Diode (SPAD) detector which can be used to trigger the collection of the photons in the Intensified CCD (ICCD) camera. The images obtained that are shown in Fig. 2 were taken with 0.5 s exposure accumulated over 300 frames.



Supplementary Figure S1. Simplified schematic of the experimental setup for Quantum Ghost Imaging. A 1 GHz, 100 fs laser is used to pump a nonlinear crystal (BBO) for second harmonic generation. The second harmonic beam is used to pump a Type-I bismuth triborate (BiBO) crystal for entangled photon pair generation. One of the photons is sent to a Spatial Light Modulator, a liquid crystal device, on which images of human faces are superposed with a diffraction grating. The second photon is sent to a camera through an image preserving delay line where the image of the object is formed. Figure legends: BiBO - 0.5-mm-thick bismuth triborate crystal; BS - Beamsplitter; BS - Beam splitter; SPAD - Single Photon Avalanche Diode; ICCD - Intensified CCD camera.



Supplementary Figure S2. Quantum circuit for the trace calculation of sparse matrix.

S2. QUANTUM COMPUTATION OF TRACE

Here, we suggest an adder algorithm [44] to compute the trace of a matrix via adding the diagonal elements of the matrix A . This operator is mainly based on quantum Fourier transform (QFT) and inverse QFT (i.e. QFT^{-1}). The algorithm should process the binary forms of the diagonal. For example, the binary representation of the diagonal elements a_{11} and a_{22} of matrix A are respectively $a_{11} = \alpha_1 2^{n-1} + \alpha_2 2^{n-2} + \dots + \alpha_n 2^0$ and $a_{22} = \beta_1 2^{n-1} + \beta_2 2^{n-2} + \dots + \beta_n 2^0$, which are $|a_{11}\rangle = |\alpha_1\rangle \otimes |\alpha_2\rangle \otimes \dots \otimes |\alpha_n\rangle$ and $|a_{22}\rangle = |\beta_1\rangle \otimes |\beta_2\rangle \otimes \dots \otimes |\beta_n\rangle$ in the form of quantum kets. The QFT operation on binary state is $\text{QFT}|a\rangle = \frac{1}{\sqrt{N}} \sum_{k=0}^{N-1} e^{\frac{i2\pi ak}{N}} |k\rangle$ and the operation of QFT^{-1} is $\text{QFT}^{-1}|k\rangle = \frac{1}{\sqrt{N}} \sum_{a=0}^{N-1} e^{-\frac{i2\pi ak}{N}} |a\rangle$ [44]. For simplicity, we introduce a representation for QFT as

$$|\Phi(a)\rangle = \text{QFT}|a\rangle = \frac{1}{\sqrt{N}} \sum_{k=0}^{N-1} e^{\frac{i2\pi ak}{N}} |k\rangle,$$

so, we can write

$$\text{QFT}^{-1}|\Phi(a)\rangle = \text{QFT}^{-1}\text{QFT}|a\rangle = |a\rangle.$$

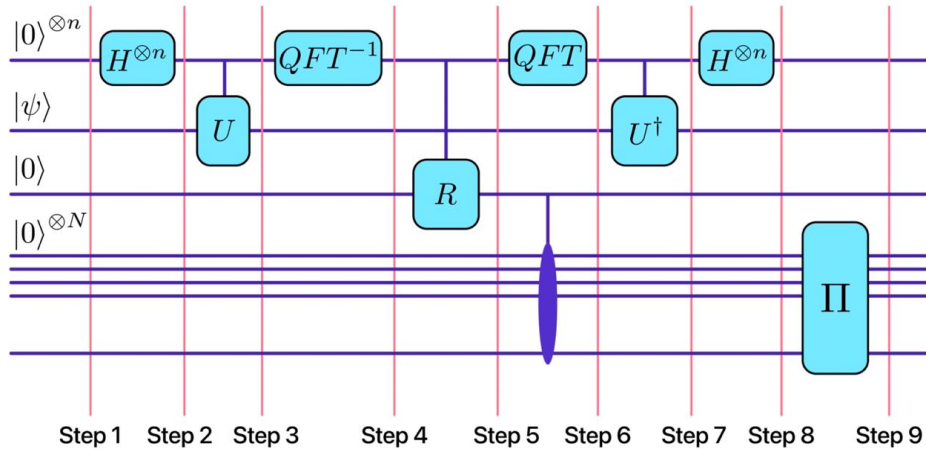
In order to calculate the trace, we need to add all diagonal elements $|a_{11}\rangle + |a_{22}\rangle + \dots + |a_{NN}\rangle$ to have the ket include the value of trace as $|a_{11} + a_{22} + \dots + a_{NN}\rangle$. We introduce the operator Σ that adds two elements a_{11} and a_{22} in the form of $|a_{11} + a_{22}\rangle$ as follows:

$$\Sigma(|a_{11}\rangle|\Phi(a_{22})\rangle) = |\Phi(a_{11} + a_{22})\rangle.$$

Then, after the operation of QFT^{-1} we obtain

$$\text{QFT}^{-1}(|\Phi(a_{11} + a_{22})\rangle) = |a_{11} + a_{22}\rangle.$$

By continuation of this method for the all diagonal elements, the trace can be obtained. The quantum protocol for computation of trace is depicted in Fig. S2, in which the input is $|a_{11}\rangle|a_{22}\rangle \dots |a_{NN}\rangle$ and the output is $|\Phi(a_{11} + a_{22} + \dots + a_{NN})\rangle = |\Phi(\text{Tr}(A))\rangle$. Finally, by an operation of QFT^{-1} we can get $|\text{Tr}(A)\rangle$. The whole process based on QFT and QFT^{-1} has a complexity $\log N$.



Supplementary Figure S3. Quantum circuit of determinant calculation of sparse matrix

S3. QUANTUM COMPUTATION OF SPARSE MATRIX DETERMINANTS

Our algorithm for computation of determinant is clarified in the following subsections as inputs, algorithm boxes, and algorithm steps:

1. Inputs

- Sparse matrix A
- $|0\rangle^{\otimes n}|\Psi\rangle$ as the input in QPE
- $|0\rangle$ as the ancilla for rotation operator
- $|0\rangle^{\otimes N}$ as the memory register for multiplication operator

2. Algorithm Boxes

- QPE is the quantum phase estimation subroutine composed of $H^{\otimes n}$, CU (i.e. controlled-U) and inverse quantum Fourier transform (QFT^{-1})
- Rotation operation (\mathbb{R})
- $(QPE)^{-1}$ is the inverse operation of QPE, composed of $H^{\otimes n}$, CU^\dagger and quantum Fourier transform (QFT)
- Π is a multiplication operation

The matrix A can be exponentiated as the unitary operator $U = e^{\frac{2\pi i A}{2^n}}$ with logarithmic complexity [7] in which n is the precision. This unitary operator is used in the controlled-U (i.e. CU) part of QPE, and $|\Psi\rangle$ is the superposition of the eigenvectors of A in the form of $|\Psi\rangle = \sum \beta_j |u_j\rangle$. Figure S3 is the representation of the quantum protocol for the computation of matrix determinants. The following steps are based on the steps shown in Fig. S3.

STEP 1:

The initial state of the algorithm is:

$$|0\rangle^{\otimes n}|\Psi\rangle|0\rangle|0\rangle^{\otimes N}. \quad (S1)$$

STEP 2:

After the operation of n Hadamard gates, i.e. $H^{\otimes n}$, we have:

$$\frac{1}{2^{\frac{n}{2}}} \sum_{y_1, \dots, y_n=0}^1 |y_1 \dots y_n\rangle |\Psi\rangle |0\rangle |0\rangle^{\otimes N}. \quad (S2)$$

STEP 3:

In this step, let us apply the controlled-U (CU) operation:

$$\frac{1}{2^{\frac{n}{2}}} \sum_{y=0}^{2^n-1} \sum_{j=1}^N \beta_j e^{\frac{2\pi i \lambda_j y}{2^n}} |y\rangle |u_j\rangle |0\rangle |0\rangle^{\otimes N}, \quad (\text{S3})$$

where $y = \sum_{l=1}^n y_l 2^{n-l}$ and λ_j 's are the eigenvalues of matrix A .

STEP 4:

Here, we apply the inverse Fourier Transform,

$$\frac{1}{2^n} \sum_{y=0}^{2^n-1} \sum_{k=0}^{2^n-1} \sum_{j=1}^N \beta_j e^{2\pi i \left(\frac{\lambda_j - k}{2^n}\right) y} |k\rangle |u_j\rangle |0\rangle |0\rangle^{\otimes N}. \quad (\text{S4})$$

For a single k among the all possible values, we have $\lambda_j - k = 0$, where $\lambda_j = x = k$. The other terms will be set to zero. Thus, the notation k is changed to the notation x :

$$\frac{1}{2^n} \sum_{y=0}^{2^n-1} e^{2\pi i \left(\frac{\lambda_j - x}{2^n}\right) y} = 1 \quad (\text{S5})$$

In this case, the state becomes:

$$\sum_{x=0}^{2^n-1} \sum_{j=1}^N \beta_j |\lambda_j\rangle |u_j\rangle |0\rangle |0\rangle^{\otimes N} = \sum_{x_1 \dots x_n=0}^1 \sum_{j=1}^N \beta_j |x_1 x_2 \dots x_n\rangle |u_j\rangle |0\rangle |0\rangle^{\otimes N},$$

where

$$\lambda_j = \sum_{l=0}^n x_l 2^{n-l} = 2^n \sum_{l=0}^n x_l 2^{-l} = 2^n \tilde{\lambda}_j.$$

STEP 5:

In this step, we apply the rotation operation $\mathbb{R}_l = e^{\frac{i\sigma_y}{2^l}}$, where σ_y is the Pauli matrix y , which acts on the output of QFT⁻¹:

$$\sum_{x_1 \dots x_n=0}^1 \sum_{j=1}^N \beta_j |x_1 \dots x_n\rangle |u_j\rangle (\sqrt{1 - \tilde{\lambda}_j^2} |0\rangle + \tilde{\lambda}_j |1\rangle). \quad (\text{S6})$$

STEP 6:

Applying the quantum Fourier transform (QFT) results in:

$$\frac{1}{2^{\frac{n}{2}}} \sum_{y=0}^{2^n-1} \sum_{j=1}^N \beta_j e^{\frac{2\pi i \lambda_j y}{2^n}} |y\rangle |u_j\rangle (\sqrt{1 - \tilde{\lambda}_j^2} |0\rangle + \tilde{\lambda}_j |1\rangle). \quad (\text{S7})$$

STEP 7:

In this step, we apply the CU^\dagger operator,

$$\frac{1}{2^{\frac{n}{2}}} \sum_{y=0}^{2^n-1} \sum_{j=1}^N \beta_j |y\rangle |u_j\rangle (\sqrt{1 - \tilde{\lambda}_j^2} |0\rangle + \tilde{\lambda}_j |1\rangle). \quad (\text{S8})$$

STEP 8:

As $|u_j\rangle$'s are known, we repeat the algorithm N times, each time for a specific $|u_j\rangle$, and consequently we obtain the following state:

$$|0\rangle^{\otimes n} |\Psi\rangle \prod_{j=1}^n (\sqrt{1 - \tilde{\lambda}_j^2} |0\rangle + \tilde{\lambda}_j |1\rangle). \quad (\text{S9})$$

Now, the goal is to measure the multiplication of $\tilde{\lambda}_j$'s in the output of multiplication operation;

$$\begin{aligned} \prod_j^N \left(\sqrt{1 - \tilde{\lambda}_j^2} |0\rangle + \tilde{\lambda}_j |1\rangle \right) &= \left(\sqrt{1 - \tilde{\lambda}_1^2} |0\rangle + \tilde{\lambda}_1 |1\rangle \right) \dots \left(\sqrt{1 - \tilde{\lambda}_N^2} |0\rangle + \tilde{\lambda}_N |1\rangle \right) \quad (\text{S10}) \\ &= \left(\sqrt{1 - \tilde{\lambda}_1^2} \right) \dots \left(\sqrt{1 - \tilde{\lambda}_N^2} \right) |00 \dots 0\rangle + \left(\sqrt{1 - \tilde{\lambda}_1^2} \right) (\tilde{\lambda}_2) \dots |0100 \dots 0\rangle + \dots + \overbrace{(\tilde{\lambda}_1)(\tilde{\lambda}_2) \dots (\tilde{\lambda}_N)}^{\tilde{\lambda}_1 \dots \tilde{\lambda}_N} \overbrace{|111 \dots 1\rangle}^N. \quad (\text{S11}) \end{aligned}$$

The coefficient of the state $|\underbrace{11 \dots 1}_N\rangle$ is the term $\tilde{\lambda}_1 \tilde{\lambda}_2 \dots \tilde{\lambda}_N$ in the output of the multiplier, which can be obtained via a weak measurement without collapsing other lines. As $\lambda_j = 2^n \tilde{\lambda}_j$, we can obtain the determinant of A (i.e. $\lambda_1 \lambda_2 \dots \lambda_N$) via relation $(2^n)^N \tilde{\lambda}_1 \tilde{\lambda}_2 \dots \tilde{\lambda}_N = \lambda_1 \lambda_2 \dots \lambda_N = \det(A)$.

A. Proof of the steps

The proof for each of the eight steps, described above, are given in details in the following expressions.

STEP 2:

$$\begin{aligned} |\Psi_2\rangle &= (H_2^{\otimes n} \otimes \mathbb{1}_N \otimes \mathbb{1}_2 \otimes \mathbb{1}_2^{\otimes N}) |0\rangle^{\otimes n} |\Psi\rangle |0\rangle |0\rangle^{\otimes N} = \frac{1}{2^{\frac{n}{2}}} \sum_{y=0}^{2^n-1} |y\rangle |\Psi\rangle |0\rangle |0\rangle^{\otimes N} \\ &= \frac{1}{2^{\frac{n}{2}}} \sum_{y_1 \dots y_n=0}^1 |y_1 \dots y_n\rangle |\Psi\rangle |0\rangle |0\rangle^{\otimes N} \quad (\text{S12}) \end{aligned}$$

STEP 3:

$$\begin{aligned} |\Psi_3\rangle &= \prod_{l=1}^n (\mathbb{1}_2^{\otimes l-1} \otimes |0\rangle\langle 0| \otimes \mathbb{1}_2^{\otimes n-l} \otimes \mathbb{1}_N \otimes \mathbb{1}_2 \otimes \mathbb{1}_2^{\otimes N} + \mathbb{1}_2^{\otimes l-1} \otimes |1\rangle\langle 1| \otimes \mathbb{1}_2^{\otimes n-l} \otimes U^{2^{n-l}} \otimes \mathbb{1}_2 \otimes \mathbb{1}_2^{\otimes N}) \frac{1}{2^{\frac{n}{2}}} \times \\ &\times \sum_{y_1 \dots y_n=0}^1 |y_1 \dots y_n\rangle \sum_{j=1}^N \beta_j |u_j\rangle |0\rangle |0\rangle^{\otimes N} \\ &= \frac{1}{2^{\frac{n}{2}}} \sum_{y_1 \dots y_n=0}^1 \sum_{j=1}^N \beta_j \prod_{l=1}^n (\text{CU})_l |y_1 \dots y_n\rangle |u_j\rangle |0\rangle |0\rangle^{\otimes N} \\ &= \frac{1}{2^{\frac{n}{2}}} \left(\sum_{y_1 \dots y_n=0}^1 \sum_{j=1}^N \beta_j \prod_{l=1}^n (\delta_{0,y_l} + \delta_{1,y_l} e^{2\pi i \tilde{\lambda}_j 2^{n-l}}) |y_1 \dots y_n\rangle |u_j\rangle |0\rangle |0\rangle^{\otimes N} \right) \\ &= \frac{1}{2^{\frac{n}{2}}} \left(\sum_{y_1 \dots y_n=0}^1 \sum_{j=1}^N \beta_j \prod_{l=1}^n e^{2\pi i \tilde{\lambda}_j y_l 2^{n-l}} |y_1 \dots y_n\rangle |u_j\rangle |0\rangle |0\rangle^{\otimes N} \right) \\ &= \frac{1}{2^{\frac{n}{2}}} \left(\sum_{y_1 \dots y_n=0}^1 \sum_{j=1}^N \beta_j e^{2\pi i \tilde{\lambda}_j \sum_{l=1}^n y_l 2^{n-l}} |y_1 \dots y_n\rangle |u_j\rangle |0\rangle |0\rangle^{\otimes N} \right) \\ &= \frac{1}{2^{\frac{n}{2}}} \sum_{y=0}^{2^n-1} \sum_{j=1}^N \beta_j e^{2\pi i \tilde{\lambda}_j y} |y\rangle |u_j\rangle |0\rangle |0\rangle^{\otimes N} \quad (\text{S13}) \end{aligned}$$

STEP 4:

$$\begin{aligned}
|\Psi_4\rangle &= (\text{QFT}^{-1} \otimes \mathbb{1}_N \otimes \mathbb{1}_2 \otimes \mathbb{1}_2^{\otimes N}) \frac{1}{2^{\frac{n}{2}}} \sum_{y=0}^{2^n-1} \sum_{j=1}^N \beta_j e^{2\pi i \tilde{\lambda}_j y} |y\rangle |u_j\rangle |0\rangle |0\rangle^{\otimes N} \\
&= \frac{1}{2^{\frac{n}{2}}} \sum_{y=0}^{2^n-1} \sum_{j=1}^N \beta_j e^{2\pi i \tilde{\lambda}_j y} (\text{QFT}^{-1} |y\rangle) |u_j\rangle |0\rangle |0\rangle^{\otimes N} \\
&= \frac{1}{2^{\frac{n}{2}}} \sum_{y=0}^{2^n-1} \sum_{j=1}^N \beta_j e^{2\pi i \tilde{\lambda}_j y} \left(\frac{1}{2^{\frac{n}{2}}} \sum_{k=0}^{2^n-1} e^{-2\pi i \frac{k}{2^n} y} |k\rangle \langle y| \right) |u_j\rangle |0\rangle |0\rangle^{\otimes N} \\
&= \frac{1}{2^n} \sum_{y=0}^{2^n-1} \sum_{k=0}^{2^n-1} \sum_{j=1}^N \beta_j e^{2\pi i (\tilde{\lambda}_j - \frac{k}{2^n}) y} |k\rangle |u_j\rangle |0\rangle |0\rangle^{\otimes N} \\
&= \frac{1}{2^n} \sum_{y=0}^{2^n-1} \sum_{k=0}^{2^n-1} \sum_{j=1}^N \beta_j e^{2\pi i (\frac{\lambda_j - k}{2^n}) y} |k\rangle |u_j\rangle |0\rangle |0\rangle^{\otimes N}
\end{aligned} \tag{S14}$$

$$|\Psi_4\rangle = \sum_{x=0}^{2^n-1} \sum_{j=1}^N \beta_j |\lambda_j\rangle |u_j\rangle |0\rangle |0\rangle^{\otimes N} = \sum_{x_1 \dots x_n=0}^1 \sum_{j=1}^N \beta_j |x_1 x_2 \dots x_n\rangle |u_j\rangle |0\rangle |0\rangle^{\otimes N} \tag{S15}$$

STEP 5:

$$\begin{aligned}
|\Psi_5\rangle &= \prod_{l=1}^n (\mathbb{1}_2^{\otimes n-l+1} \otimes |0\rangle \langle 0| \otimes \mathbb{1}_2^{\otimes l} \otimes \mathbb{1}_N \otimes \mathbb{1}_2 \otimes \mathbb{1}_2^{\otimes N} + \mathbb{1}_2^{\otimes n-l+1} \otimes |1\rangle \langle 1| \otimes \mathbb{1}_2^{\otimes l} \otimes \mathbb{1}_N \otimes \mathbb{R}_{n-l}) \otimes \mathbb{1}_2^{\otimes N} \times \\
&\times \sum_{x_1 \dots x_n=0}^1 |x_1 \dots x_n\rangle \sum_{j=1}^N \beta_j |u_j\rangle |0\rangle \\
&= \sum_{x_1 \dots x_n=0}^1 \sum_{j=1}^N \beta_j \prod_{l=1}^n (\text{CR})_{n-l+1} |x_1 \dots x_n\rangle |u_j\rangle |0\rangle |0\rangle^{\otimes N} \\
&= \sum_{x_1 \dots x_n=0}^1 \sum_{j=1}^N \beta_j |x_1 \dots x_n\rangle |u_j\rangle \left(\prod_{l=1}^n (\delta_{0, x_{n-l+1}} + \delta_{1, x_{n-l+1}} e^{\frac{i\sigma_y}{2^{n-l+1}}}) |0\rangle \right) |0\rangle^{\otimes N} \\
&= \sum_{x_1 \dots x_n=0}^1 \sum_{j=1}^N \beta_j |x_1 \dots x_n\rangle |u_j\rangle \left(\prod_{l=1}^n e^{i\sigma_y x_{n-l+1} 2^{-(n-l+1)}} |0\rangle \right) |0\rangle^{\otimes N} \\
&= \sum_{x_1 \dots x_n=0}^1 \sum_{j=1}^N \beta_j |x_1 \dots x_n\rangle |u_j\rangle (e^{i\sigma_y \sum_{l=1}^n x_{n-l+1} 2^{-(n-l+1)}} |0\rangle) |0\rangle^{\otimes N} \\
&= \sum_{x_1 \dots x_n=0}^1 \sum_{j=1}^N \beta_j |x_1 \dots x_n\rangle |u_j\rangle (e^{i\sigma_y \tilde{\lambda}_j} |0\rangle) |0\rangle^{\otimes N}.
\end{aligned} \tag{S16}$$

STEP 6:

$$\begin{aligned}
|\Psi_6\rangle &= (\text{QFT} \otimes \mathbb{1}_N \otimes \mathbb{1}_2 \otimes \mathbb{1}_2^{\otimes N}) \sum_{x_1 \dots x_n=0}^1 \sum_{j=1}^N \beta_j |x_1 \dots x_n\rangle |u_j\rangle (\sqrt{1 - \tilde{\lambda}_j^2} |0\rangle + \tilde{\lambda}_j |1\rangle) \\
&= (\text{QFT} \sum_{x_1 \dots x_n=0}^1 |x_1 \dots x_n\rangle) \sum_{j=1}^N \beta_j |u_j\rangle (\sqrt{1 - \tilde{\lambda}_j^2} |0\rangle + \tilde{\lambda}_j |1\rangle) \\
&= \left(\frac{1}{2^{\frac{n}{2}}} \sum_{y=0}^{2^n-1} e^{2\pi i \frac{k}{2^n} y} |y\rangle \langle k| \sum_{x_1 \dots x_n=0}^1 |x_1 \dots x_n\rangle\right) \sum_{j=1}^N \beta_j |u_j\rangle (\sqrt{1 - \tilde{\lambda}_j^2} |0\rangle + \tilde{\lambda}_j |1\rangle) \\
&= \left(\frac{1}{2^{\frac{n}{2}}} \sum_{y=0}^{2^n-1} e^{2\pi i \frac{k}{2^n} y} |y\rangle \sum_{x_1 \dots x_n=0}^1 \langle k|x_1 \dots x_n\rangle\right) \sum_{j=1}^N \beta_j |u_j\rangle (\sqrt{1 - \tilde{\lambda}_j^2} |0\rangle + \tilde{\lambda}_j |1\rangle) \\
&= \left(\frac{1}{2^{\frac{n}{2}}} \sum_{y=0}^{2^n-1} e^{2\pi i \frac{k}{2^n} y} |y\rangle \sum_{x_1 \dots x_n=0}^1 \delta_{k, x_1 \dots x_n}\right) \sum_{j=1}^N \beta_j |u_j\rangle (\sqrt{1 - \tilde{\lambda}_j^2} |0\rangle + \tilde{\lambda}_j |1\rangle) \\
&= \left(\frac{1}{2^{\frac{n}{2}}} \sum_{y=0}^{2^n-1} e^{2\pi i \frac{k}{2^n} y} |y\rangle \delta_{k, \lambda_j}\right) \sum_{j=1}^N \beta_j |u_j\rangle (\sqrt{1 - \tilde{\lambda}_j^2} |0\rangle + \tilde{\lambda}_j |1\rangle) \\
&= \frac{1}{2^{\frac{n}{2}}} \sum_{y=0}^{2^n-1} e^{2\pi i \frac{\lambda_j}{2^n} y} |y\rangle \sum_{j=1}^N \beta_j |u_j\rangle (\sqrt{1 - \tilde{\lambda}_j^2} |0\rangle + \tilde{\lambda}_j |1\rangle) \\
&= \frac{1}{2^{\frac{n}{2}}} \sum_{y=0}^{2^n-1} \sum_{j=1}^N \beta_j e^{2\pi i \frac{\lambda_j}{2^n} y} |y\rangle |u_j\rangle (\sqrt{1 - \tilde{\lambda}_j^2} |0\rangle + \tilde{\lambda}_j |1\rangle)
\end{aligned} \tag{S17}$$

STEP 7:

$$\begin{aligned}
|\Psi_7\rangle &= \prod_{l=1}^n (\mathbb{1}_2^{\otimes l-1} \otimes |0\rangle \langle 0| \otimes \mathbb{1}_2^{\otimes n-l} \otimes \mathbb{1}_N \otimes \mathbb{1}_2 \otimes \mathbb{1}_2^{\otimes N} + \mathbb{1}_2^{\otimes l-1} \otimes |1\rangle \langle 1| \otimes \mathbb{1}_2^{\otimes n-l} \otimes (U^\dagger)^{2^{n-l}} \otimes \mathbb{1}_2 \otimes \mathbb{1}_2^{\otimes N}) \times \\
&\times \frac{1}{2^{\frac{n}{2}}} \sum_{y=0}^{2^n-1} \sum_{j=1}^N \beta_j e^{2\pi i \frac{\lambda_j}{2^n} y} |y\rangle |u_j\rangle (\sqrt{1 - \tilde{\lambda}_j^2} |0\rangle + \tilde{\lambda}_j |1\rangle) \\
&= \frac{1}{2^{\frac{n}{2}}} \sum_{y_1 \dots y_n=0}^1 \sum_{j=1}^N \beta_j e^{2\pi i \frac{\lambda_j}{2^n} y} \prod_{l=1}^n (\text{CU}^\dagger)_l |y_1 \dots y_n\rangle |u_j\rangle (\sqrt{1 - \tilde{\lambda}_j^2} |0\rangle + \tilde{\lambda}_j |1\rangle) \\
&= \frac{1}{2^{\frac{n}{2}}} \left(\sum_{y_1 \dots y_n=0}^1 \sum_{j=1}^N \beta_j e^{2\pi i \frac{\lambda_j}{2^n} y} \prod_{l=1}^n (\delta_{0, y_l} + \delta_{1, y_l} e^{-2\pi i \lambda_j 2^{n-l}}) |y_1 \dots y_n\rangle |u_j\rangle (\sqrt{1 - \tilde{\lambda}_j^2} |0\rangle + \tilde{\lambda}_j |1\rangle) \right) \\
&= \frac{1}{2^{\frac{n}{2}}} \left(\sum_{y_1 \dots y_n=0}^1 \sum_{j=1}^N \beta_j e^{2\pi i \frac{\lambda_j}{2^n} y} \prod_{l=1}^n e^{-2\pi i \lambda_j y_l 2^{n-l}} |y_1 \dots y_n\rangle |u_j\rangle (\sqrt{1 - \tilde{\lambda}_j^2} |0\rangle + \tilde{\lambda}_j |1\rangle) \right) \\
&= \frac{1}{2^{\frac{n}{2}}} \left(\sum_{y_1 \dots y_n=0}^1 \sum_{j=1}^N \beta_j e^{2\pi i \frac{\lambda_j}{2^n} y} e^{-2\pi i \lambda_j \sum_{l=1}^n y_l 2^{n-l}} |y_1 \dots y_n\rangle |u_j\rangle (\sqrt{1 - \tilde{\lambda}_j^2} |0\rangle + \tilde{\lambda}_j |1\rangle) \right) \\
&= \frac{1}{2^{\frac{n}{2}}} \left(\sum_{y_1 \dots y_n=0}^1 \sum_{j=1}^N \beta_j e^{2\pi i \frac{\lambda_j}{2^n} y} e^{-2\pi i \tilde{\lambda}_j y} |y_1 \dots y_n\rangle |u_j\rangle (\sqrt{1 - \tilde{\lambda}_j^2} |0\rangle + \tilde{\lambda}_j |1\rangle) \right) \\
&= \frac{1}{2^{\frac{n}{2}}} \sum_{y=0}^{2^n-1} \sum_{j=1}^N \beta_j e^{\frac{2\pi i}{2^n} (\lambda_j - \tilde{\lambda}_j) y} |y\rangle |u_j\rangle (\sqrt{1 - \tilde{\lambda}_j^2} |0\rangle + \tilde{\lambda}_j |1\rangle) \\
&= \frac{1}{2^{\frac{n}{2}}} \sum_{y=0}^{2^n-1} \sum_{j=1}^N \beta_j |y\rangle |u_j\rangle (\sqrt{1 - \tilde{\lambda}_j^2} |0\rangle + \tilde{\lambda}_j |1\rangle).
\end{aligned} \tag{S18}$$

STEP 8:

$$\begin{aligned}
|\Psi_8\rangle &= (H_2^{\otimes n} \otimes \mathbb{1}_N \otimes \mathbb{1}_2 \otimes \mathbb{1}_2^{\otimes N}) \frac{1}{2^{\frac{n}{2}}} \sum_{y=0}^{2^n-1} \sum_{j=1}^N \beta_j |y\rangle |u_j\rangle (\sqrt{1-\tilde{\lambda}_j^2} |0\rangle + \tilde{\lambda}_j |1\rangle) \\
&= |0\rangle^{\otimes n} \sum_{j=1}^N \beta_j |u_j\rangle (\sqrt{1-\tilde{\lambda}_j^2} |0\rangle + \tilde{\lambda}_j |1\rangle) \tag{S19}
\end{aligned}$$

$$\begin{aligned}
\prod_j^N (\sqrt{1-\tilde{\lambda}_j^2} |0\rangle + \tilde{\lambda}_j |1\rangle) &= (\sqrt{1-\tilde{\lambda}_1^2} |0\rangle + \tilde{\lambda}_1 |1\rangle) \dots (\sqrt{1-\tilde{\lambda}_N^2} |0\rangle + \tilde{\lambda}_N |1\rangle) \\
&= (\sqrt{1-\tilde{\lambda}_1^2}) \dots (\sqrt{1-\tilde{\lambda}_N^2}) |00\dots 0\rangle + (\sqrt{1-\tilde{\lambda}_1^2}) (\tilde{\lambda}_2) \dots |0100\dots 0\rangle + \dots + \overbrace{(\tilde{\lambda}_1)(\tilde{\lambda}_2) \dots (\tilde{\lambda}_N)}^{\tilde{\lambda}_1 \dots \tilde{\lambda}_N} \overbrace{|111\dots 1\rangle}^N \tag{S20}
\end{aligned}$$